Mon. Not. R. Astron. Soc. **368,** 325–334 (2006) doi:10.1111/j.1365-2966.2006.10097.x

Gemini/GMOS spectra of globular clusters in the Virgo giant elliptical NGC 4649

Michael Pierce,[1⋆] Terry Bridges,[2] Duncan A. Forbes,[1] Robert Proctor,[1] Michael A. Beasley,[3] Karl Gebhardt,[4] Favio Raul Faifer,[5,6] Juan Carlos Forte,[5] Stephen E. Zepf,[7] Ray Sharples[8] and David A. Hanes[2]

[1]*Centre for Astrophysics & Supercomputing, Swinburne University, Hawthorn, VIC 3122, Australia*
[2]*Department of Physics, Queen's University, Kingston, ON K7L 3N6, Canada*
[3]*Lick Observatory, University of California, Santa Cruz, CA 95064, USA*
[4]*Astronomy Department, University of Texas, Austin, TX 78712, USA*
[5]*Facultad de Cs. Astronomicas y Geofisicas, UNLP, Paseo del Bosque 1900, La Plata, and CONICET, Argentina*
[6]*IALP - CONICET, Argentina*
[7]*Department of Physics and Astronomy, Michigan State University, East Lansing, MI 48824, USA*
[8]*Department of Physics, University of Durham, South Road, Durham DH1 3LE*

Accepted 2006 January 24. Received 2006 January 23; in original form 2006 January 14

ABSTRACT

NGC 4649 (M60) is one of a handful of giant Virgo ellipticals. We have obtained Gemini/GMOS (Gemini North Multi-Object Spectrograph) spectra for 38 globular clusters (GCs) associated with this galaxy. Applying the multi-index χ^2 minimization technique of Proctor and Sansom with the single stellar population models of Thomas, Maraston and Korn, we derive ages, metallicities and α-element abundance ratios. We find several young (2–3 Gyr old) supersolar metallicity GCs, while the majority are old (>10 Gyr), spanning a range of metallicities from solar to [Z/H] = −2. At least two of these young GCs are at large projected radii of 17–20 kpc. The galaxy itself shows no obvious signs of a recent starburst, interaction or merger. A trend of decreasing α-element ratio with increasing metallicity is found.

Key words: globular clusters: general – galaxies: individual: NGC 4649 – galaxies: star clusters.

1 INTRODUCTION

Accurately determined ages, metallicities and α-element abundances of globular cluster (GC) systems across the entire range of galaxy types can provide strong constraints for galaxy formation models. One example of such a constraint is the recently observed trend of decreasing α/Fe ratios with increasing metallicity for extragalactic GC systems (Pierce et al. 2005, 2006; Puzia et al. 2005). This trend restricts the allowable chemical enrichment histories, relative contribution of Type Ia versus Type II supernova and star formation time-scales for galaxies well beyond the Local Group, where there is little possibility of directly resolving stellar populations.

To accurately measure ages, metallicities and abundance ratios with Lick indices from low-resolution spectra require a minimum signal-to-noise ratio (S/N) of ∼30, which corresponds to an Hβ error of ±0.3 Å (Cardiel et al. 2003). With an integration time of ∼8 h on an 8-m class telescope, it is possible to obtain multi-object spectra to this depth for the brightest GCs of a rich GC system for galaxies within ∼20 Mpc of the Milky Way.

⋆E-mail: mpierce@astro.swin.edu.au

A major aim of most moderate to high S/N GC spectroscopy has been to measure ages and hence infer when GC formation occurred. Spectroscopic follow-up is a complimentary approach to recent photometric results. Rhode, Zepf & Santos (2005) show that the mass-normalized number of blue GCs increases with host galaxy mass. This suggests that the formation of blue GCs is affected by the mass of the host halo. The observed 'blue tilt' correlation between GC luminosity and colour of the blue, metal-poor, subpopulation (Strader et al. 2005; Harris et al. 2006) requires significant spectroscopic follow-up to be both confirmed and understood. Another property of the blue subpopulation to be studied is the correlation between host galaxy luminosity and mean blue GC subpopulation colour (Strader, Brodie & Forbes 2004b), which implies a correlation between galaxy mass and blue GC metallicity. This is another indication that the formation of blue GCs is affected by the mass of the host halo.

The majority of the most recent GC spectroscopy for large ellipticals has focused on group ellipticals (e.g. NGC 1052, Pierce et al. 2005; NGC 3379, Pierce et al. 2006; NGC 3610, Strader et al. 2003; Strader, Brodie & Forbes 2004a; NGC 5128, Peng, Ford & Freeman 2004; NGC 2434, 3379, 3585, 5846 and 7192, Puzia et al. 2004).

From the literature, there are several large ellipticals in clusters for which GC spectra have been analysed to measure ages and metallicities. Cohen, Blakeslee & Ryzhov (1998) present spectral indices for 150 of M87's GCs. These vary in S/N, with a sizeable fraction of high enough quality to be useful. Co-adding GCs of similar metallicity, they find the GCs are generally old ($\geqslant$10 Gyr) with metallicities spanning from [Fe/H] $= -2$ to above solar. Cohen, Blakeslee & Côté (2003) measure metallicities for 47 GCs associated with NGC 4472 (M49). However, the S/N is less than 30 for all of the spectra and therefore ages for individual GCs cannot be measured with any confidence. Beasley et al. (2000) co-added spectra for NGC 4472 GCs finding both the metal-rich and metal-poor subpopulations to be old.

For the Fornax cluster, Kissler-Patig et al. (1998) measured metallicities for 18 GCs around NGC 1399. Forbes et al. (2001) presented higher S/N spectra for 10 GCs and found two to be young (1–2 Gyr). From the Goudfrooij et al. (2001) spectroscopic sample of NGC 1316, only the spectra of three exceptionally bright GCs have high enough S/N to measure ages. The Lick indices of all three bright GCs indicate a young age ($\sim$3 Gyr) corresponding to the host galaxy's recent merger event. The GC colour–magnitude plot for NGC 1316 is atypical in that there is a significant population of bright, intermediate-colour GCs.

One galaxy with what appears to be conflicting results is NGC 4365 in the Virgo cluster. Brodie et al. (2005) present spectroscopic results for NGC 4365 GCs and find some GCs, previously thought to belong to an intermediate age subpopulation (Puzia et al. 2002; Larsen et al. 2003), are in fact an intermediate metallicity subpopulation with old ages. Kundu et al. (2005) present *Hubble Space Telescope* NIC3 *H*-band data, and find that these agree with earlier claims of a GC subpopulation with intermediate ages 2–8 Gyr. There appears to be no consensus yet for the GC population of this galaxy, unlike other systems.

While possessing a larger GC population, cD and brightest cluster galaxies have the additional complication of GCs potentially associated with the cluster potential. The Virgo cluster elliptical NGC 4649 (M60) is a worthy target for GC spectroscopy as a non-central, giant, cluster elliptical.

NGC 4649 (M60) is luminous, $M_V = -22.38$ and relatively nearby at $D = 16.8$ Mpc. Ultraviolet (UV) data for the galaxy light suggest a major old population, plus minor ongoing star formation (Magris & Bruzual 1993). However, from optical spectra, Terlevich & Forbes (2002) measure Lick indices and obtain an age of 11 Gyr, metallicity of [Fe/H] $= +0.3$ and [Mg/Fe] $= +0.3$ for the central regions of the galaxy. The *Chandra* X-ray observations of Randall, Sarazin & Irwin (2004) find some structure in the diffuse gas.

The GC imaging study of Forbes et al. (2004) found the standard colour bimodality and $S_N = 4.1$. Assuming the two subpopulations have similar mass functions, this suggests a similar formation age. NGC 4649 is one of the galaxies with the observed 'blue tilt' (Strader et al. 2005). Recently, Spitler et al. (2006) have shown that the 'blue tilt' is present amongst the GC population of a nearby spiral galaxy, the Sombrero. Unfortunately, our spectroscopic sample does not sample far enough down the luminosity function to adequately test hypotheses regarding the 'blue tilt'.

2 OBSERVATIONS AND DATA REDUCTION

The observations described below are part of Gemini program GN-2002A-Q-13. GC candidates were selected from Gemini North Multi-Object Spectrograph (GMOS; Hook et al. 2002) imaging,obtained during 2002 April, for three fields around NGC 4649. The data reduction and GC candidate selection process is described in Forbes et al. (2004) and Bridges et al. (2006).

GMOS masks for three fields were designed, but only the central field was observed within the time allocated. Spectra of NGC 4649 GCs were obtained with GMOS on the Gemini North telescope during 2003 on May 31, June 1, 4 and 27. Seeing ranged from 0.65–0.9 arcsec over the four nights. Exposures of 16×1800 s were taken, yielding a total of 8-h on-source integration time. Bias frames, dome flat-fields and copper–argon (CuAr) arc exposures were taken as part of the Gemini baseline calibrations. From the CuAr arcs, wavelength solutions with typical residuals of 0.1 Å were achieved.

These data were reduced using the GEMINI/GMOS packages in IRAF and a number of custom made scripts (see Bridges et al. 2006 for details). After some experimentation, optimal (variance) extraction was found to yield the best results since our data are oversampled on the detector. In some cases, objects were too faint to trace individually and we therefore co-added several 2D images, taken adjacent in time, to act as a reference for the extractions. We verified beforehand that flexure was minimal between the reference images. Finally, the extracted spectra were median combined and weighted by their fluxes with cosmic ray rejection.

In the absence of any velocity standard stars, the recession velocities were measured by using six Bruzual & Charlot (2003) model stellar energy distributions (SEDs) for 14 and 5 Gyr ages with metallicities [Fe/H] $= -1.64$, -0.33 and $+0.1$. The task FXCOR in IRAF was used and the average was taken. Objects with recession velocities in the range $1100 \pm 600\,\mathrm{km\,s^{-1}}$ are potentially associated with NGC 4649. These are presented in Table 1. There was one background object (a quasi-stellar object at $z \sim 0.5$) out of the 39 spectra obtained. Our low contamination rate of 2.5 per cent is due to good imaging and colour selection.

In order to measure Lick indices, we convolved our spectra with a wavelength-dependent Gaussian kernel to match the resolution of the Lick/IDS (Image-Dissector Scanner) system (see Beasley et al. 2004b). Lick indices (Trager et al. 1998) were measured from our spectra. Due to the variable wavelength ranges in these spectra,the same set of indices could not be measured for all spectra. However, all covered a wavelength range of 4500–5500 Å. Uncertainties in the indices were derived from the photon noise in the unfluxed spectra. No Lick standard stars were observed, so we cannot fully calibrate the GCs on to the Lick system (see Pierce et al. 2006). Consequently, there are some small systematic differences between some of the measured indices and those used in the single stellar population (SSP) models. These issues are discussed further in Sections 3 and 4. Measured line indices are presented in Tables 2 and 3. Line index uncertainties are presented in Tables 4 and 5. The final spectra have S/N = 5–21 $\mathrm{Å^{-1}}$ at 5000 Å, giving errors in the Hβ index of 0.12–0.38 Å.

3 AGES, METALLICITIES AND α-ELEMENT ABUNDANCE RATIOS

In this section, we describe the measurement of ages, metallicities and α-element abundances which are presented in Table 6. We apply the χ^2 multi-index fitting technique of Proctor & Sansom (2002) for this analysis. This method involves the comparison of the measured Lick indices with SSP models (its application to extragalactic GCs is described fully in Pierce et al. 2005, 2006). The SSP models of Thomas, Maraston & Korn (2004, hereafter TMK04) were chosen because these include the effect of α abundance ratios on the Balmer lines, unlike the models of Bruzual & Charlot (2003) and Vazdekis (1999).

Table 1. Confirmed GCs around NGC 4649. Cluster ID, coordinates, g magnitude and $g - i$ colours are from our GMOS imaging and are instrumental magnitudes only. Heliocentric velocities are from the spectra presented in this work.

ID	RA (J2000) (h m s)	Dec. (J2000) (° ′ ″)	X (pixel)	Y (pixel)	g (mag)	$g - i$ (mag)	$V_{\rm helio}$ (km s^{-1})	$V_{\rm err}$ (km s^{-1})
89	12:43:56.15	11:32:12.26	1324.96	478.67	22.72	1.08	1199.2	43.4
124	12:43:55.45	11:32:12.38	1339.40	621.02	21.91	0.88	833.4	59.6
68	12:43:56.68	11:32:21.90	1447.41	362.65	22.58	1.22	649.3	33.6
148	12:43:54.49	11:32:42.55	1769.64	777.98	22.74	1.14	1184.8	46.8
175	12:43:53.86	11:31:54.28	1120.73	961.31	22.29	1.18	852.3	37.6
183	12:43:53.43	11:32:18.65	1461.97	1019.24	22.26	1.13	1299.4	35.8
158	12:43:53.17	11:35:20.76	3957.80	853.95	23.21	1.16	1261.0	46.0
360	12:43:47.94	11:35:40.01	4316.58	1883.79	21.20	0.91	1270.1	40.1
329	12:43:49.83	11:32:18.93	1531.35	1741.23	21.93	0.88	1511.2	65.3
277	12:43:51.06	11:32:53.22	1978.06	1454.03	22.59	1.04	1299.1	46.5
251	12:43:50.43	11:35:59.83	4542.24	1358.58	22.29	1.09	1099.7	43.9
298	12:43:50.48	11:33:05.25	2153.17	1556.03	22.58	0.90	1063.0	52.5
318	12:43:50.23	11:32:11.63	1424.30	1671.14	23.08	1.00	1173.4	48.6
606	12:43:44.82	11:32:54.60	2110.58	2706.89	21.36	1.18	627.0	39.6
558	12:43:45.23	11:33:18.50	2430.02	2595.52	21.75	0.74	1087.8	50.8
434	12:43:47.83	11:31:43.07	1077.12	2185.82	22.18	1.04	925.9	36.6
462	12:43:47.33	11:31:56.43	1269.20	2272.22	22.18	0.92	1112.8	45.4
517	12:43:56.16	11:32:20.79	1623.47	2476.30	22.03	1.14	857.2	56.3
412	12:43:47.00	11:34:57.45	3751.32	2121.39	22.48	0.95	483.6	47.5
502	12:43:46.23	11:33:34.66	2632.89	2375.35	22.10	1.17	688.6	43.5
640	12:43:43.48	11:35:09.77	3984.06	2815.36	22.61	0.79	1015.5	104.5
740	12:43:43.71	11:31:44.88	1176.86	3012.11	21.68	0.98	962.1	44.8
806	12:43:43.03	11:32:20.30	1673.81	3107.00	21.50	1.18	1197.4	46.2
899	12:43:42.54	11:32:01.70	1428.31	3227.10	21.44	0.92	1372.0	42.7
975	12:43:41.90	11:32:20.48	1696.82	3333.25	20.99	0.92	1052.2	42.3
1063	12:43:40.99	11:32:09.49	1563.10	3529.46	21.37	0.94	953.9	47.3
1011	12:43:40.38	11:35:47.99	4563.36	3393.26	21.95	0.94	1135.0	45.7
1037	12:43:40.69	11:33:51.36	2962.26	3469.39	21.97	1.13	667.9	63.4
1145	12:43:39.98	11:31:58.76	1434.77	3745.73	21.60	1.08	1017.1	42.6
1252	12:43:38.55	11:32:39.51	2018.25	3985.40	21.27	0.89	926.8	47.3
1384	12:43:37.51	11:33:03.43	2364.45	4165.70	20.91	1.03	1134.2	47.0
1126	12:43:40.43	11:31:33.69	1083.67	3685.07	22.21	0.90	1122.0	58.2
1298	12:43:38.28	11:32:09.97	1619.00	4073.00	22.25	1.13	1346.1	47.9
1211	12:43:38.89	11:32:41.10	2033.87	3914.83	22.29	1.01	1324.5	38.0
1098	12:43:39.56	11:34:52.00	3812.20	3623.63	22.27	0.77	889.3	69.3
1182	12:43:38.82	11:33:46.70	2932.52	3850.43	22.32	1.15	1305.2	39.3
1574	12:43:35.18	11:36:09.38	4950.56	4411.99	21.65	1.01	1454.0	45.1
1443	12:43:37.20	11:33:05.80	2402.56	4225.51	22.65	1.28	703.0	53.9

We compare the measured Lick indices to the TMK04 SSPs and obtain a minimum χ^2 fit. This fit is initially sought using all the indices measured. Simultaneously, a set of χ^2 minimization fits are found with each of the indices omitted. From this set, we select the fit with the lowest total χ^2, remove the necessary index and repeat until a stable fit is achieved with no highly aberrant ($>4\sigma$) indices remaining. All GCs had some indices that were significant outliers to the fit and therefore removed during this process. The errors given for the derived parameters are statistical 1σ confidence intervals calculated by a Monte Carlo style method (see Proctor, Forbes & Beasley 2004; Pierce et al. 2005, for details).

The molecular band indices $\rm Mg_1$ and $\rm Mg_2$ are systematically offset due a number of calibration issues and were excluded for all GCs (see Proctor et al. 2005; Pierce et al. 2006). Similar to other GC studies (e.g. Beasley et al. 2004a), we find the CN indices to be enhanced relative to the models and therefore they were also removed.

From our sample of 38 GCs, eight had poor or uncertain fits. We will identify these with open symbols in all figures. In particular, GC 640 is found to be very metal-poor. We find a Brodie–Huchra (Brodie & Huchra 1990) metallicity of -2.6 dex, which is 0.85 dex lower than any other GC in this sample. Many of the metal-sensitive indices are below the values spanned by the SSP grids. One consequence of the low [Fe/H] is a high [E/Fe] uncertainty.

For GC 1443, there exists a conflict between the indices Fe4531, Fe5270 and Fe5335 which suggest a low metallicity and Fe4383, C4668, Fe5406, Fe5015 and Mgb which suggest the GC has super-solar metallicity. We find the more compelling fit is for a young and super metal-rich GC, however, this result is uncertain. Neither the Brodie–Huchra metallicity nor the photometric colours offer any strong constraint.

Low S/N makes a stable fit difficult for GCs 158 and 318. The inclusion or exclusion of single indices, that are well below any clipping threshold, can change the resulting fit. GC 318 is potentially part of the so-called 'H' GC subpopulation noted by Strader et al. (2005) of intermediate colour GCs, at approximately the turn-over magnitude. GC 158 is in the magnitude range as well, but is too red to be considered a part of this subpopulation.

Table 2. GC indices $\lambda < 4600$ Å. Indices in brackets are removed during the fitting process. Missing values are due to limited wavelength coverage. Index errors are presented in Table 4.

ID	$H\delta_A$ (Å)	$H\delta_F$ (Å)	CN_1 (mag)	CN_2 (mag)	Ca4227 (Å)	G band (Å)	$H\gamma_A$ (Å)	$H\gamma_F$ (Å)	Fe4383 (Å)	Ca4455 (Å)	Fe4531 (Å)
89	(−8.936)	(−0.154)	(0.125)	(0.165)	0.448	5.290	−1.691	0.944	2.259	1.085	1.939
124	3.226	2.950	(−0.008)	(0.035)	0.621	(3.662)	1.155	2.004	1.883	0.008	1.310
68	(2.165)	(3.963)	(0.033)	(0.101)	1.045	5.253	−5.858	−0.766	(8.650)	2.139	(5.030)
148	(−10.481)	(−3.591)	(0.295)	(0.357)	1.440	(2.541)	(−3.292)	(0.473)	6.518	0.823	3.553
175	(−2.707)	(−0.900)	(0.168)	(0.173)	1.016	2.234	−2.255	−0.180	2.729	2.310	3.974
183	0.270	0.831	(0.083)	(0.051)	−0.004	5.785	−3.500	−0.165	4.196	1.225	2.247
158	−3.139	−0.488	(0.180)	(0.151)	0.882	6.213	−1.419	0.893	3.112	1.406	3.244
360	–	–	–	–	0.865	3.528	−1.488	0.556	2.904	1.068	2.187
329	1.989	1.520	(−0.085)	(−0.078)	0.305	(1.784)	−0.260	0.830	2.898	0.702	0.928
277	(0.415)	(2.965)	(−0.070)	(−0.041)	0.614	4.777	−6.229	−2.614	4.175	0.609	2.223
251	–	–	–	–	–	6.561	−4.919	−1.155	2.320	(0.087)	2.617
298	3.471	(−1.123)	(−0.137)	(−0.142)	(−1.050)	0.375	(3.654)	(3.162)	1.359	(1.426)	0.426
318	(−6.529)	(−2.985)	(0.181)	(0.190)	1.187	4.917	0.321	1.237	−1.053	0.943	(6.004)
606	−0.875	0.697	(0.145)	(0.197)	(0.401)	5.062	−5.650	−1.572	4.103	1.209	3.229
558	3.361	2.874	(−0.061)	(−0.030)	0.183	(3.782)	1.268	(3.135)	(3.474)	0.382	1.311
434	−0.600	−0.655	(0.027)	(0.060)	0.182	6.155	−4.006	−1.522	(0.478)	0.618	2.909
462	0.503	2.451	(0.096)	(0.122)	1.444	5.113	−3.244	−0.350	0.392	0.793	2.908
517	(4.415)	(4.534)	(0.043)	(0.033)	(−0.051)	4.880	−3.174	−0.156	2.425	1.193	2.759
412	0.235	0.859	(−0.054)	(−0.072)	(−0.867)	4.880	−3.487	0.392	2.514	1.509	1.864
502	(−4.873)	(−1.419)	(0.209)	(0.225)	1.121	5.483	−4.837	−0.666	4.282	(0.933)	4.245
640	(1.353)	(1.588)	(0.035)	(0.052)	(2.221)	0.728	(6.237)	3.149	−4.268	1.415	0.314
740	2.822	3.308	(0.011)	(0.027)	0.617	3.172	−0.098	1.478	2.720	0.625	1.785
806	(−5.422)	(−1.911)	(0.302)	(0.361)	1.077	(3.982)	−6.102	−0.699	6.163	1.663	3.206
899	1.250	1.462	(0.024)	(0.068)	0.831	4.754	−2.170	0.321	2.233	0.133	2.367
975	3.233	2.390	(−0.030)	(0.022)	0.478	3.632	−0.767	0.980	1.782	0.150	2.049
1063	0.349	1.798	(0.028)	(0.057)	0.076	2.937	−1.370	1.176	3.206	0.733	1.619
1011	–	–	–	–	–	(5.206)	−1.727	(1.520)	3.486	(−0.183)	2.550
1037	−0.260	−1.406	(0.148)	(0.202)	(0.405)	(1.864)	(−2.044)	−0.808	3.080	0.460	4.094
1145	−0.414	0.605	(0.083)	(0.107)	0.635	5.077	−3.217	−0.668	2.842	1.186	2.451
1252	1.541	2.265	(0.048)	(0.076)	0.694	3.673	−1.594	0.725	2.029	0.125	1.823
1384	(−0.236)	(1.215)	(0.068)	(0.092)	0.618	3.596	−1.039	0.727	1.054	0.569	2.381
1126	(−1.003)	(1.215)	(0.078)	(0.105)	0.032	(2.886)	1.166	2.330	(5.764)	1.223	0.288
1298	(−3.213)	(1.650)	(0.131)	(0.179)	0.643	5.052	−3.889	−0.447	4.607	1.422	2.993
1211	(−2.832)	(0.173)	(0.222)	(0.245)	1.118	4.989	−2.369	0.862	2.320	0.751	1.741
1098	2.101	1.964	(0.002)	(0.018)	(−1.346)	3.909	1.203	1.692	−0.399	−0.643	1.470
1182	−1.099	0.500	(0.204)	(0.231)	0.705	3.754	−4.786	−0.178	5.309	0.547	1.187
1574	–	–	–	–	–	–	–	–	–	0.443	2.740
1443	(−8.897)	(−2.203)	(0.250)	(0.350)	1.441	3.752	−4.720	−0.683	5.693	(−1.506)	(0.000)

For GC 298, Hβ and Hγ suggest different ages (similar to the Galactic GC NGC 6171, see Proctor et al. 2004). The metal-sensitive indices suggest that this GC is metal-poor and therefore more likely to be older than 5 Gyr.

The *Hubble Space Telescope* Advance Camera for Surveys (*HST*/ACS) images (Proposal 9401, see Bridges et al., in preparation) show GC 558 is extended and therefore is possibly a stripped dwarf. The χ^2 fit for 558 gives an old, metal-poor population with an apparently negative [E/Fe]. If this really is a stripped dwarf, we do not necessarily expect to be able to fit it with a single stellar population due to potential stellar population gradients. We note that there are complex issues with sky subtraction around Mgb for this object on some nights; therefore Mgb is not included in the fit for this object.

We find two GCs, 517 and 1182, which appear to be of intermediate age ∼5 Gyr. Both are around solar metallicity ([Z/H] ∼ 0), but with differing [E/Fe] (+0.3 versus −0.06). It is not clear whether these GCs are in fact intermediate aged or if the age–metallicity degeneracy is not broken effectively in these cases.

The three clearly young and metal-rich GCs are 89, 175 and 502; these will be shown as squares on all plots. Their α-element abundance ratios are all [E/Fe] ∼ 0.3 within errors. It is interesting to note that these GCs are not amongst the brightest objects in our sample. All three are observed to be photometrically red. See Section 4, for more on the young GCs.

In summary (see Fig. 1), within errors, we find that the majority of GCs are consistent with an old age ($\geqslant$10 Gyr). There are two GCs with potentially intermediate ages ∼5 Gyr, three GCs that are definitely young (2–3 Gyr) and another GC that is most likely young.

One means to test our SSP-derived metallicities is to compare them with those derived by the Brodie & Huchra (1990; BH) method, which was originally calibrated to old stellar populations. Fig. 2 shows good agreement for the SSP-derived metallicities of old GCs and estimates from the BH method. One would expect the BH method to give lower metallicities for young stellar populations. However, the 'young' objects (ages <5 Gyr), while systematically offset from the one-to-one line by ∼0.5 dex, are within the scatter of the full sample.

Table 3. GC indices $\lambda > 4600$ Å. Indices in brackets are removed during the fitting process. Missing values are due to limited wavelength coverage. Index errors are presented in Table 5.

ID	C4668 (Å)	Hβ (Å)	Fe5015 (Å)	Mg$_1$ (mag)	Mg$_2$ (mag)	Mgb (Å)	Fe5270 (Å)	Fe5335 (Å)	Fe5406 (Å)	Fe5709 (Å)	Fe5782 (Å)
89	3.089	(0.060)	6.110	(0.022)	(0.140)	3.582	1.318	2.239	1.677	–	–
124	−0.554	2.540	2.414	(−0.023)	(0.055)	1.740	1.433	1.686	0.771	–	–
68	3.689	1.188	(2.959)	(0.030)	(0.207)	3.641	2.867	(3.201)	1.719	–	–
148	4.343	1.559	5.026	(0.021)	(0.125)	3.140	2.632	1.258	1.386	–	–
175	6.261	1.336	4.277	(0.079)	(0.209)	3.148	2.794	2.074	1.612	–	–
183	0.592	2.337	4.266	(0.021)	(0.149)	3.265	2.208	1.830	1.233	–	–
158	2.391	0.326	3.733	(0.010)	(0.147)	3.022	2.638	1.438	1.376	0.823	1.039
360	2.034	2.574	3.346	(0.011)	(0.093)	2.057	1.726	1.386	1.017	0.549	0.248
329	1.044	2.401	3.422	(−0.018)	(0.059)	1.844	1.085	0.730	0.342	–	–
277	1.967	0.693	3.140	(0.047)	(0.148)	3.575	2.039	1.968	1.142	–	–
251	3.537	1.213	5.896	(0.060)	(0.221)	4.205	1.952	2.026	1.621	0.600	0.666
298	−0.013	2.302	2.896	(0.019)	(0.037)	1.072	(1.647)	1.052	1.083	–	–
318	(−5.908)	0.490	−1.582	(−0.032)	(0.093)	2.665	−0.015	2.098	1.380	–	–
606	4.089	1.486	4.178	(0.102)	(0.242)	3.531	(1.912)	(2.670)	(1.665)	–	–
558	−1.369	2.326	2.665	(0.010)	(0.044)	(0.671)	1.889	1.503	0.607	–	–
434	2.491	1.878	2.343	(0.025)	(0.123)	2.506	2.118	1.852	0.903	–	–
462	2.792	1.203	(2.264)	(0.023)	(0.104)	2.234	2.104	0.806	0.988	–	–
517	4.152	(1.208)	4.771	(0.080)	(0.201)	3.094	(3.386)	1.581	1.391	–	–
412	3.400	(0.110)	3.138	(0.041)	(0.106)	2.258	(0.861)	2.101	1.017	0.451	0.812
502	7.967	2.025	6.563	(0.107)	(0.287)	5.055	2.396	3.027	1.513	0.555	–
640	2.724	2.310	0.315	(−0.055)	(−0.067)	(−0.753)	−0.508	1.176	(−0.343)	0.189	(0.752)
740	0.912	1.340	(4.897)	(0.010)	(0.109)	2.759	1.770	1.713	0.935	–	–
806	4.799	0.995	(2.748)	(0.076)	(0.282)	(5.771)	2.819	2.265	1.744	–	–
899	1.132	1.847	2.220	(0.002)	(0.090)	2.692	1.416	(1.844)	0.903	–	–
975	0.648	2.222	3.512	(−0.004)	(0.083)	2.330	1.691	1.420	0.711	–	–
1063	2.715	2.109	3.420	(−0.008)	(0.086)	1.769	1.693	1.530	0.959	–	–
1011	3.098	1.602	2.698	(0.072)	(0.135)	(1.685)	1.984	0.972	1.159	0.508	0.430
1037	(5.808)	1.082	5.031	(0.078)	(0.233)	3.307	2.351	1.509	(−0.189)	(−0.008)	0.410
1145	3.328	1.800	5.140	(0.041)	(0.182)	3.746	2.080	1.744	1.449	–	–
1252	0.854	2.480	4.032	(−0.016)	(0.084)	(1.908)	1.484	1.480	0.726	–	–
1384	(4.074)	1.862	2.771	(0.059)	(0.150)	2.590	1.839	1.390	(1.181)	–	–
1126	0.487	2.999	1.284	(−0.013)	(0.065)	1.288	0.919	0.772	0.099	–	–
1298	1.132	1.634	2.884	(0.014)	(0.141)	3.575	1.882	1.781	0.972	–	–
1211	1.910	1.433	2.478	(0.036)	(0.192)	(2.128)	2.149	(2.962)	(1.666)	–	–
1098	−1.524	(0.813)	2.016	(−0.038)	(0.041)	2.144	1.139	0.298	−0.282	0.883	0.180
1182	5.486	1.656	5.991	(0.103)	(0.257)	(5.120)	1.632	2.840	1.048	(1.795)	0.985
1574	0.993	1.899	3.024	(0.031)	(0.109)	(2.388)	1.254	0.543	1.067	0.395	0.328
1443	6.813	1.976	(8.367)	(0.028)	(0.217)	(5.264)	(0.929)	(1.110)	2.288	–	–

A clear trend of decreasing [E/Fe] with increasing [Fe/H] is seen in Fig. 3. For GCs associated with NGC 3379, Pierce et al. (2006) used the index–index plots to confirm the suggestion of a trend in the χ^2 fit α-element abundances. Similar index–index plots for NGC 4649 GCs do not show the trend that is seen in the fitted parameters. In the case presented here, there is the added complication of age differences between GCs, whereas the NGC 3379 GCs of Pierce et al. (2006) were found to be universally old. It should be noted that we find no trend of α-element abundance ratios with age.

4 DISCUSSION

One of the more important factors for the χ fitting analysis used in this work is the determination of errors. Uncertainties in the background subtraction of sky and galaxy light introduce Lick index errors in addition to the easily quantifiable Poisson noise. The relative effect of these errors increases for fainter GCs, so in reality not only do fainter GCs have larger index errors, but also those errors are increasingly underestimated.

Assuming Gaussian errors due to photon noise, 95 per cent of measurements should be within 2σ. For most objects, we measure $\sim$16 indices, which means that when we apply a 2σ clip, only 1 index measurement should be excluded on average per object. For the application of χ^2 fitting to extragalactic GCs, this is clearly not the case as we are often forced to exclude three to seven indices at greater than 3σ before a stable result is obtained. Here, we are also assuming that the SSP models are perfect. Both flux calibration and calibration to the Lick system introduce further errors and uncertainties.

The main manifestation of these unaccounted for errors is the increased difficulty in constraining ages and α-element abundance ratios for fainter GCs. In general, metallicities are less susceptible to these effects because of the large number (>10) of predominantly metallicity sensitive indices available. By contrast, there are only three primarily age indicators (i.e. the Hβ, Hγ and Hδ lines) and only a few strongly sensitive α-element indices.

This underestimation of errors probably occurs in all extragalactic GC samples. For example, the large and homogeneous sample of Puzia et al. (2004) has index errors that appear underestimated by

Table 4. GC indices errors $\lambda < 4600$ Å. Missing values are due to limited wavelength coverage. Index errors are derived from photon noise in the unfluxed spectra.

ID	$H\delta_A$ (Å)	$H\delta_F$ (Å)	CN_1 (mag)	CN_2 (mag)	Ca4227 (Å)	G band (Å)	$H\gamma_A$ (Å)	$H\gamma_F$ (Å)	Fe4383 (Å)	Ca4455 (Å)	Fe4531 (Å)
89	0.822	0.472	0.017	0.020	0.322	0.500	0.539	0.328	0.731	0.356	0.530
124	0.375	0.253	0.011	0.013	0.204	0.341	0.336	0.208	0.494	0.252	0.368
68	0.594	0.365	0.017	0.019	0.305	0.492	0.572	0.345	0.616	0.326	0.466
148	0.851	0.554	0.018	0.021	0.309	0.551	0.566	0.336	0.686	0.369	0.519
175	0.606	0.413	0.015	0.018	0.261	0.472	0.458	0.293	0.610	0.281	0.420
183	0.515	0.353	0.014	0.016	0.271	0.399	0.455	0.281	0.571	0.284	0.418
158	0.989	0.649	0.024	0.028	0.436	0.656	0.729	0.459	0.971	0.478	0.667
360	–	–	–	–	0.160	0.273	0.281	0.175	0.383	0.188	0.280
329	0.397	0.279	0.011	0.013	0.212	0.367	0.351	0.223	0.494	0.245	0.371
277	0.597	0.368	0.016	0.019	0.304	0.505	0.579	0.381	0.692	0.353	0.515
251	–	–	–	–	–	0.433	0.524	0.331	0.673	0.332	0.459
298	0.499	0.421	0.015	0.017	0.321	0.493	0.429	0.263	0.692	0.325	0.514
318	0.730	0.504	0.018	0.021	0.325	0.562	0.582	0.366	0.888	0.428	0.570
606	0.384	0.257	0.010	0.012	0.181	0.284	0.323	0.204	0.389	0.193	0.277
558	0.364	0.246	0.011	0.012	0.201	0.328	0.321	0.187	0.454	0.236	0.351
434	0.514	0.378	0.013	0.015	0.248	0.371	0.438	0.286	0.599	0.286	0.403
462	0.488	0.310	0.013	0.015	0.220	0.383	0.424	0.267	0.581	0.279	0.406
517	0.496	0.312	0.014	0.016	0.267	0.387	0.428	0.266	0.569	0.278	0.394
412	0.561	0.386	0.015	0.018	0.318	0.460	0.519	0.312	0.690	0.328	0.485
502	0.625	0.414	0.014	0.017	0.248	0.401	0.458	0.283	0.557	0.278	0.391
640	0.579	0.400	0.016	0.018	0.263	0.522	0.424	0.279	0.798	0.351	0.560
740	0.362	0.235	0.010	0.012	0.194	0.318	0.317	0.195	0.448	0.228	0.332
806	0.469	0.313	0.011	0.013	0.187	0.309	0.346	0.206	0.399	0.206	0.302
899	0.336	0.231	0.009	0.011	0.167	0.276	0.298	0.186	0.404	0.204	0.291
975	0.257	0.179	0.007	0.009	0.137	0.226	0.232	0.144	0.331	0.169	0.242
1063	0.333	0.219	0.009	0.010	0.170	0.278	0.280	0.169	0.382	0.194	0.287
1011	–	–	–	–	–	0.366	0.404	0.238	0.540	0.284	0.392
1037	0.503	0.381	0.013	0.015	0.245	0.412	0.405	0.264	0.542	0.272	0.370
1145	0.401	0.274	0.010	0.012	0.189	0.302	0.334	0.214	0.435	0.212	0.313
1252	0.302	0.200	0.008	0.010	0.151	0.255	0.266	0.165	0.372	0.191	0.276
1384	0.276	0.184	0.007	0.009	0.135	0.227	0.228	0.143	0.324	0.159	0.231
1126	0.491	0.321	0.013	0.015	0.248	0.403	0.387	0.234	0.521	0.273	0.429
1298	0.572	0.340	0.014	0.016	0.259	0.410	0.458	0.285	0.568	0.283	0.421
1211	0.574	0.376	0.014	0.016	0.243	0.403	0.441	0.267	0.595	0.295	0.438
1098	0.473	0.323	0.013	0.016	0.282	0.416	0.407	0.255	0.627	0.326	0.460
1182	0.562	0.376	0.015	0.017	0.262	0.441	0.479	0.289	0.579	0.310	0.437
1574	–	–	–	–	–	–	–	–	–	0.230	0.327
1443	0.828	0.524	0.017	0.020	0.298	0.520	0.560	0.347	0.667	0.389	0.532

up to a factor of 2 based on the scatter in index–index plots. The χ^2 fitting method we apply is immune to this effect as long as the errors are uniformly underestimated by the same factor across all indices. However, it is unlikely this is the case as sky subtraction and galaxy light subtraction could affect every index differently. Despite these uncertainties, the χ^2 fitting method applied in this work appears to be robust to problems with individual indices. GCs strongly affected by error underestimation are easily identified during the fitting process. Modelling errors including horizontal branch morphology and α-element abundance prescriptions are also factors in the imperfect matching of observed data to the SSPs.

At least three, and possibly four, GCs are found to be young (2–3 Gyr old) out of our sample of 38. This proportion is similar to the two young GCs from a sample of 10 found by Forbes et al. (2001) for NGC 1399, another large cluster elliptical with no signs of recent star formation. A 2–3 Gyr old central burst of star formation that is approximately 10 per cent by mass of the underlying old 10–14 Gyr population will cause a significant change to the spectral indices of the galaxy (e.g. Proctor et al. 2005). This has not been reported for the NGC 4649 galaxy light itself. Indeed, Terlevich & Forbes (2002) find the central stellar population of NGC 4649 to be ∼11 Gyr old. There are no observations to suggest a significant recent burst of star formation in NGC 4649 (the UV SED work of Magris & Bruzual (1993) suggests minor ongoing star formation). Do these young GCs suggest that some of the GCs associated with large cluster gEs are not formed in that galaxy? Two of the young GCs (87 and 175) are at large projected galactocentric radii (see Fig. 4). These GCs are on the opposite side of NGC 4649 to the nearby companion spiral NGC 4647 (see fig. 1 of Bridges et al. 2006).

This result raises several possibilities, first that there was minimal galaxy star formation when these young GCs were formed and therefore GCs do not trace star formation particularly well. This would be contrary to what is commonly observed in other systems. Secondly, that our sampling is not representative of the overall GC population. This possibility is difficult to rule out. Thirdly, that GC accretion is a common enough process for large ellipticals that the GC system is 'contaminated' by GCs formed in other galaxies and therefore the GC system is a complex trace of a combination of star

Table 5. GC indices errors $\lambda > 4600$ Å. Missing values are due to limited wavelength coverage. Index errors are derived from photon noise in the unfluxed spectra.

ID	C4668 (Å)	Hβ (Å)	Fe5015 (Å)	Mg_1 (mag)	Mg_2 (mag)	Mgb (Å)	Fe5270 (Å)	Fe5335 (Å)	Fe5406 (Å)	Fe5709 (Å)	Fe5782 (Å)
89	0.746	0.284	0.535	0.006	0.006	0.245	0.283	0.309	0.222	–	–
124	0.539	0.186	0.393	0.004	0.005	0.179	0.199	0.224	0.165	–	–
68	0.702	0.261	0.527	0.005	0.006	0.231	0.247	0.273	0.206	–	–
148	0.743	0.277	0.566	0.006	0.007	0.253	0.278	0.324	0.234	–	–
175	0.595	0.224	0.453	0.005	0.005	0.207	0.221	0.250	0.183	–	–
183	0.615	0.213	0.443	0.004	0.005	0.201	0.220	0.251	0.182	–	–
158	1.010	0.384	0.756	0.007	0.009	0.335	0.358	0.416	0.301	0.223	0.206
360	0.405	0.144	0.307	0.003	0.004	0.139	0.153	0.173	0.127	0.095	0.090
329	0.533	0.189	0.400	0.004	0.005	0.183	0.206	0.235	0.172	–	–
277	0.734	0.272	0.558	0.005	0.006	0.239	0.266	0.302	0.223	–	–
251	0.652	0.247	0.487	0.005	0.006	0.218	0.243	0.272	0.198	0.152	0.140
298	0.737	0.257	0.549	0.005	0.006	0.254	0.272	0.319	0.229	–	–
318	0.984	0.348	0.751	0.007	0.008	0.309	0.363	0.391	0.282	–	–
606	0.406	0.149	0.311	0.003	0.004	0.140	0.152	0.166	0.123	–	–
558	0.523	0.181	0.389	0.004	0.004	0.182	0.194	0.222	0.163	–	–
434	0.584	0.209	0.446	0.004	0.005	0.201	0.221	0.249	0.184	–	–
462	0.591	0.222	0.455	0.005	0.005	0.207	0.227	0.265	0.190	–	–
517	0.563	0.212	0.422	0.004	0.005	0.190	0.199	0.232	0.169	–	–
412	0.707	0.279	0.547	0.005	0.006	0.246	0.276	0.303	0.225	0.170	0.156
502	0.548	0.209	0.424	0.004	0.005	0.192	0.215	0.235	0.174	0.131	–
640	0.774	0.283	0.621	0.006	0.007	0.285	0.316	0.349	0.262	0.188	0.173
740	0.482	0.174	0.350	0.004	0.004	0.162	0.181	0.206	0.151	–	–
806	0.433	0.164	0.341	0.003	0.004	0.141	0.160	0.180	0.131	–	–
899	0.428	0.154	0.322	0.003	0.004	0.144	0.163	0.183	0.135	–	–
975	0.354	0.125	0.262	0.003	0.003	0.118	0.132	0.150	0.110	–	–
1063	0.412	0.149	0.310	0.003	0.004	0.144	0.156	0.177	0.129	–	–
1011	0.566	0.213	0.444	0.004	0.005	0.203	0.214	0.247	0.179	0.135	0.127
1037	0.530	0.206	0.414	0.004	0.005	0.185	0.198	0.223	0.169	0.125	0.115
1145	0.446	0.164	0.330	0.003	0.004	0.150	0.168	0.190	0.137	–	–
1252	0.402	0.138	0.290	0.003	0.003	0.136	0.150	0.171	0.126	–	–
1384	0.323	0.118	0.253	0.002	0.003	0.114	0.127	0.142	0.103	–	–
1126	0.607	0.203	0.455	0.004	0.005	0.208	0.230	0.262	0.193	–	–
1298	0.617	0.223	0.458	0.004	0.005	0.198	0.224	0.252	0.186	–	–
1211	0.624	0.226	0.464	0.005	0.005	0.220	0.230	0.253	0.188	–	–
1098	0.686	0.255	0.510	0.005	0.006	0.226	0.258	0.299	0.221	0.158	0.155
1182	0.608	0.232	0.456	0.005	0.005	0.197	0.226	0.245	0.186	0.133	0.129
1574	0.483	0.174	0.369	0.004	0.004	0.166	0.185	0.213	0.150	0.114	0.106
1443	0.692	0.263	0.504	0.005	0.006	0.230	0.280	0.311	0.218	–	–

formation and galaxy assembly. More accurate ages and α-element abundance ratios are necessary to distinguish between local formation of the young GCs in massive ellipticals or accretion from nearby galaxies with more recent star formation.

Our plot of α-element ratio with metallicity (Fig. 3) is the most visually compelling indication of a trend of decreasing [E/Fe] with increasing [Fe/H] in the literature to date. A similar trend is seen less clearly in Pierce et al. (2005) for NGC 1052 GCs, Puzia et al. (2005) for a subsample of bright GCs from five galaxies and Pierce et al. (2006) for NGC 3379 GCs.

Not all observers find the same trend in α-element ratios. Strader et al. (2004a) examine NGC 3610 GCs and appear to find an inverse trend to that presented in our Fig. 3. Based on a comparison of Mgb versus $\langle$Fe$\rangle$, they find the majority of GCs to have solar or subsolar α-element ratios. Four of the metal-rich GCs appear to have abundance ratios of +0.3 dex; interestingly, two of these are old and two are young.

Olsen et al. (2004), with a sample of six GCs associated with Sculptor group galaxies, find four metal-poor ([Fe/H] < -1) GCs with abundance ratios around [α/Fe] $= -0.3$ and two metal-poor GCs with approximately solar abundances (see fig. 8 of Olsen et al. 2004). This is derived from the ratio of Mgb/$\langle$Fe$\rangle$. We suggest, based on their fig. 6, that the calibration to the Lick system of Mgb and Fe5335 for their data may be a problem.

It is worth noting that α-element abundance ratios are poorly constrained for low metallicities, and it is therefore possible to argue that within errors the current larger samples, Pierce et al. (2005, 2006) and Puzia et al. (2005), are consistent with a universal value of [E/Fe] $= +0.3$ (consistent with Galactic α/Fe measures). The majority of GCs with well-constrained α-element abundance ratios are relatively consistent with this value within errors. The trend seen in all three data sets may then be attributed to modelling effects in the Thomas et al. (2004) models used for all these cases.

A rough order of magnitude estimate can be made of the S/N required to differentiate the α-element abundance ratios of metal-poor GCs. The expected difference in Mgb between solar abundance and [E/Fe] $= +0.3$, for a 10 Gyr [Fe/H] $= -1$ TMK04 model, is

Table 6. Derived GC properties. Age, [Fe/H], [E/Fe] and [Z/H] are derived from the χ^2 minimization process, with errors derived by a Monte Carlo style method. $[Fe/H]_{BH}$ is derived according to the method of Brodie & Huchra (1990) from a reduced sample of indices.

ID	Age (Gyr)	[Fe/H] (dex)	[E/Fe] (dex)	[Z/H] (dex)	$[Fe/H]_{BH}$ (dex)	Notes
89	2.4±0.6	−0.29±0.15	0.36±0.07	0.05±0.11	−0.86	
124	15±6.0	−1.23±0.16	0.00±0.20	−1.23±0.12	−1.60	
68	15±4.4	−0.29±0.13	0.12±0.11	−0.18±0.08	−0.53	
148	14.1±5.1	−0.34±0.13	0.12±0.10	−0.23±0.09	−1.13	
175	2.4±0.4	0.04±0.11	0.12±0.09	0.15±0.09	−0.51	
183	8.9±2.7	−0.63±0.12	0.32±0.10	−0.33±0.11	−0.73	
158	7.9±3.6	−0.45±0.21	0.18±0.18	−0.28±0.17	−0.78	Low S/N
360	7.1±2.1	−0.87±0.11	0.21±0.07	−0.68±0.11	−1.32	
329	11.9±2.1	−1.47±0.15	0.42±0.15	−1.08±0.09	−1.55	
277	15±2.7	−0.50±0.12	0.24±0.10	−0.28±0.07	−0.75	
251	15±2.7	−0.58±0.10	0.46±0.08	−0.15±0.07	−0.34	
298	15±6.5	−1.14±0.22	−0.30±0.18	−1.43±0.15	−1.74	NGC 6171 analogue
318	12.6±4.4	−1.75±0.20	0.80±0.14	−1.00±0.17	−1.41	Low S/N
606	15±2.4	−0.45±0.10	0.24±0.07	−0.23±0.05	−0.33	
558	15±6.1	−1.02±0.15	−0.30±0.15	−1.30±0.11	−1.25	Stripped dwarf?
434	12.6±2.6	−0.60±0.12	0.21±0.08	−0.40±0.09	−0.63	
462	12.6±3.7	−1.03±0.13	0.46±0.09	−0.60±0.12	−0.90	
517	5.6±1.7	−0.46±0.15	0.30±0.10	−0.18±0.10	−0.70	
412	7.9±3.2	−0.57±0.16	0.18±0.13	−0.40±0.16	−1.07	
502	3.0±0.8	0.17±0.11	0.38±0.05	0.53±0.11	−0.39	
640	13.3±4.6	−2.83±0.40	0.80±0.38	−2.08±0.25	−2.60	Very low metallicity
740	15±5.4	−1.33±0.14	0.40±0.10	−0.95±0.12	−1.14	
806	11.2±2.1	−0.10±0.09	−0.03±0.11	−0.13±0.08	−0.13	
899	11.9±2.1	−1.25±0.11	0.53±0.10	−0.75±0.08	−1.13	
975	15±4.7	−1.32±0.09	0.42±0.08	−0.93±0.06	−1.19	
1063	7.5±2.4	−0.72±0.13	−0.09±0.12	−0.80±0.10	−1.22	
1011	15±4.1	−1.01±0.14	0.36±0.24	−0.68±0.18	−0.66	
1037	15±2.9	−0.58±0.12	0.30±0.09	−0.30±0.07	−0.43	
1145	8.4±1.8	−0.53±0.09	0.38±0.06	−0.18±0.06	−0.69	
1252	8.4±2.3	−1.08±0.11	0.30±0.10	−0.80±0.10	−1.53	
1384	15±5.2	−1.26±0.14	0.46±0.08	−0.83±0.12	−0.95	
1126	8.9±2.5	−2.18±0.28	0.59±0.24	−1.63±0.19	−1.63	
1298	15±3.5	−0.82±0.12	0.42±0.10	−0.43±0.09	−0.89	
1211	15±4.8	−1.18±0.17	0.56±0.19	−0.65±0.14	−0.74	
1098	15±2.6	−2.00±0.13	0.80±0.12	−1.25±0.08	−1.72	
1182	5.3±1.4	−0.07±0.12	−0.06±0.14	−0.13±0.09	−0.73	
1574	11.9±2.6	−1.33±0.14	0.40±0.24	−0.95±0.15	−1.23	
1443	2.1±0.6	0.57±0.16	−0.21±0.10	0.38±0.17	−1.06	Complex metal lines

0.237 Å. To be able to observe a difference of this magnitude spectra with S/N corresponding to Hβ, errors of ∼0.13 Å are required. For the sample presented here, only two GCs are sufficiently bright to reach that accuracy. Calibration to the Lick system and accurate flux calibration are necessary to make possible the detailed exploration of α-element abundance effects at low metallicities. To completely resolve the differences in α-element abundance ratios currently measured, spectra of substantially higher S/N than the current samples are required.

Considering index and index error uncertainties discussed at the beginning of this section, we suggest that further work will be necessary to confidently determine if the metallicity α-element abundance ratio trend we observe is real or if it is an artefact of SSP modelling, χ^2 fitting and observation calibrations, both flux and to the Lick system.

5 CONCLUSIONS

We present ages, metallicities and α-element abundance ratios for 38 GCs around NGC 4649 based on our Gemini/GMOS spectra. These were derived by applying the multi-index χ^2 minimization method of Proctor & Sansom (2002) to the SSP models of Thomas et al. (2004). Close agreement is found with metallicity estimates derived according to the Brodie & Huchra (1990) method, with the young GCs systematically offset by a small amount (∼0.5 dex) as expected. We find three, possibly four, GCs with ages of approximately 2 Gyr, two of these are at large galactocentric radii (17–20 kpc). The α-element abundance ratio decreases with increasing metallicity.

The young GC fraction ($\leqslant$10 per cent) is consistent with the picture presented by 'frosting' models of recent minor star formation in ellipticals (Trager et al. 2000). In this particular case, noting the large galactocentric radii of two of the young GCs and the lack of evidence for recent star formation in the galaxy itself, it is quite possible that the young subpopulation was not formed natively, but instead has been accreted.

ACKNOWLEDGMENTS

We thank the Gemini support staff for help preparing the slit mask. DAF thanks the Australian Research Council (ARC) for its financial

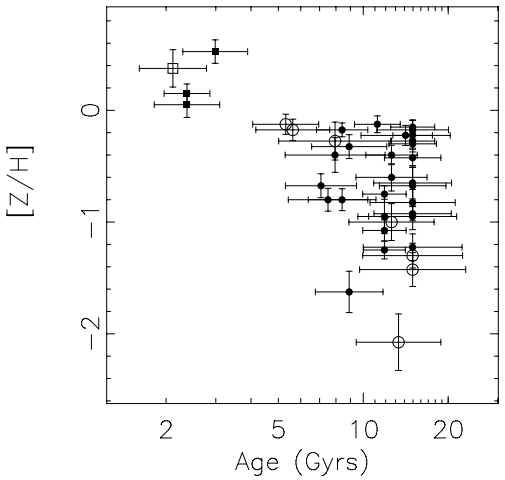

Figure 1. SSP fit metallicities and ages. GCs with uncertain fits are shown as open points. The majority of GCs are old ($\geqslant$10 Gyr) with a small number of young, very metal-rich GCs (shown as squares) and several GCs with potentially intermediate ages.

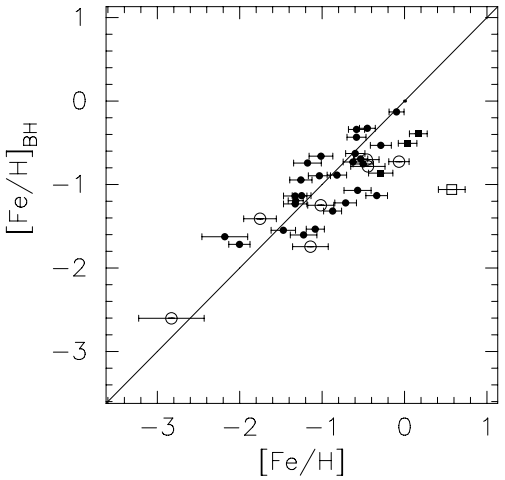

Figure 2. Brodie–Huchra metallicity is shown against SSP metallicity. The open points are GCs for which the χ^2 fits are uncertain. This plot shows a general trend of agreement for the majority of GCs. Young GCs are shown as square symbols. The clear outlier is GC 1443 where there are both strong and weak metal indices present in the spectrum.

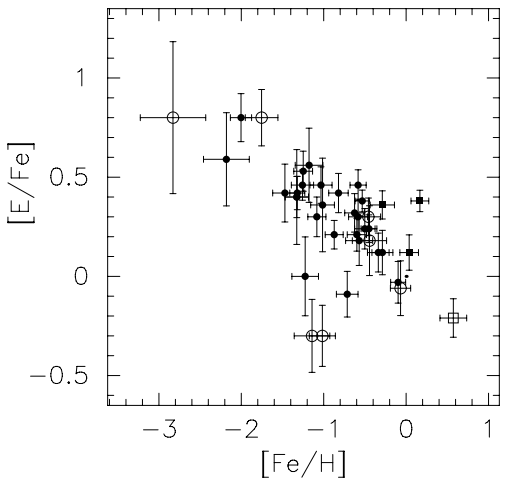

Figure 3. Alpha element abundance ratio versus metallicity. The open points are GCs for which the χ^2 fits are uncertain and the squares are young GCs. There appears to be a strong trend of decreasing [E/Fe] with increasing [Fe/H]. However, the significance of this trend is highly dependent on the low metallicity GCs ([Fe/H] <-1.5) for which [E/Fe] is very difficult to determine.

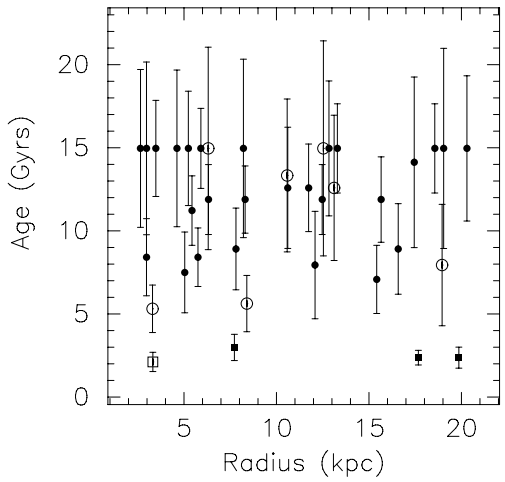

Figure 4. A plot of age versus projected galactocentric radii. The open points are GCs for which the χ^2 fits are uncertain and the squares are young GCs. There is no obvious trend with radius. Of interest are the two young GCs at large projected galactocentric radii ∼17–20 kpc.

support. SEZ acknowledges support for this work in part from the NSF grant AST-0406891 and from the Michigan State University Foundation. This research was supported in part by a discovery grant awarded to DAH by the Natural Sciences and Engineering Research Council of Canada (NSERC).

These data were based on observations obtained at the Gemini Observatory, which is operated by the Association of Universities for Research in Astronomy, Inc., under a cooperative agreement with the NSF on behalf of the Gemini partnership: the National Science Foundation (US), the Particle Physics and Astronomy Research Council (UK), the National Research Council (Canada), CONICYT (Chile), the Australian Research Council (Australia), CNPq (Brazil) and CONICET-Agencia Nac. de Promocion Cientifica y Tecnologica (Argentina). The Gemini program ID is GN-2002A-Q13. This research has made use of the NASA/IPAC Extragalactic Database (NED), which is operated by the Jet Propulsion Laboratory, Caltech, under contract with the National Aeronautics and Space Administration.

REFERENCES

Beaseley M. A., Sharples R. M., Bridges T. J., Hanes D. A., Zepf S. E., Ashman K. M., Geisler D., 2000, MNRAS, 318, 1249

Beasley M. A., Brodie J. P., Strader J., Forbes D. A., Proctor R. N., Barmby P., Huchra J. P., 2004a, AJ, 128, 1623

Beasley M. A., Forbes D. A., Brodie J. P., Kissler-Patig M., 2004b, MNRAS, 347, 1150

Bertin E., Arnouts S., 1996, A&AS, 117, 393

Bridges T. et al., 2006, MNRAS, submitted

Brodie J. P., Huchra J. P., 1990, ApJ, 362, 503 (BH)

Brodie J. P., Strader J., Denicolo G., Beasley M. A., Cenarro A. J., Larsen S. S., Kuntschner H., Forbes D. A., 2005, AJ, 129, 2643

Bruzual A. G., Charlot S., 2003, MNRAS, 344, 1000

Cardiel N., Gorgas J., Sánchez-Blázquez P., Cenarro A. J., Pedraz S., Bruzual G., Klement J., 2003, A&A, 409, 511
Cohen J. G., Blakeslee J. P., Ryzhov A. J., 1998, ApJ, 496, 808
Cohen J. G., Blakeslee J. P., Côté P., 2003, ApJ, 592, 866
Forbes D. A., Beasley M. A., Brodie J. P., Kissler-Patig M., 2001, ApJ, 563, 143
Forbes D. A. et al., 2004, MNRAS, 355, 608
Goudfrooij P., Mack J., Kissler-Patig M., Meylan G., Minniti D., 2001, MNRAS, 322, 643
Harris W. E., 1996, AJ, 112, 1487
Harris W. E., 1999, Ap&SS, 267, 95
Harris W. E., Whitmore B. C., Karakla D., Okon W., Baum W. A., Hanes D. A., Kavelaars J. J., 2006, AJ, 636, 90
Hook I. et al., 2002, SPIE, Vol. 4841, Power Telescopes and Instrumentation into the New Millennium. SPIE, Bellingham
Kissler-Patig M., Brodie J. P., Schroder L. L., Forbes D. A., Grillmair C. J., Huchra J. P., AJ, 115, 105
Kundu A. et al., 2005, ApJ, 634, L41
Larsen S. S., Brodie J. P., Beasley M. A., Forbes D. A., Kissler-Patig M., Kuntschner H., Puzia T. H., 2003, ApJ, 585, L767
Magris C. G., Bruzual A. G., 1993, ApJ, 417, 102
Olsen K. A. G., Miller B. W., Suntzeff N. B., Schommer R. A., Bright J., 2004, AJ, 127, 2674
Peng E. W., Ford H. C., Freeman K. C., 2004, ApJ, 602, 705
Pierce M. J., Brodie J. P., Forbes D. A., Beasley M. A., Proctor R. N., Strader J., 2005, MNRAS, 358, 419
Pierce M. J. et al., 2006, MNRAS, 366, 1253
Proctor R. N., Sansom A. E., 2002, MNRAS, 333, 517
Proctor R. N., Forbes D. A., Beasley M. A., 2004, MNRAS, 355, 1327
Proctor R. N., Forbes D. A., Forestell A., Gebhardt K., 2005, 362, 857
Puzia T. H., Zepf S. E., Kissler-Patig M., Hilker M., Minniti D., Goudfrooij P., 2002, A&A, 391, 453
Puzia T. H. et al., 2004, A&A, 415, 123
Puzia T. H., Kissler-Patig M., Thomas D., Maraston C., Saglia R. P., Bender R., Goudfrooij P., Hempel M., 2005, A&A, 439, 997
Randall S. W., Sarazin C. L., Irwin J. A., 2004, ApJ, 600, 729
Rhode K. L., Zepf S. E., 2004, AJ, 127, 302
Rhode K. L., Zepf S. E., Santos M. R., 2005, ApJ, 630, L21
Spitler L., Larsen S., Strader J., Brodie J., Forbes D., Beasley M., 2006, AJ, submitted
Strader J., Brodie J. P., Schweizer F., Larsen S. S., Seitzer P., 2003, AJ, 125, 626
Strader J., Brodie J. P., Forbes D. A., 2004a, AJ, 127, 295
Strader J., Brodie J. P., Forbes D. A., 2004b, AJ, 127, 3431
Strader J., Brodie J. P., Spitler L., Beasley M. A., 2005, AJ, submitted (astro-ph/0508001)
Terlevich A. I., Forbes D. A., 2002, MNRAS, 330, 547
Thomas D., Maraston C., Korn A., 2004, MNRAS, 351, 19 (TMK04)
Trager S. C., Worthey G., Faber S. M., Burstein D., Gonzalez J. J., 1998, ApJS, 116, 1
Trager S. C., Faber S. M., Worthey G., Gonzarlez J. J., 2000, AJ, 120, 165
Vazdekis A., 1999, ApJ, 513, 224

This paper has been typeset from a TEX/LATEX file prepared by the author.